JOURNAL OF THEORETICAL AND APPLIED MECHANICS
62, 1, pp. 129-142, Warsaw 2024
https://doi.org/10.15632/jtam-pl/177259

ANALYTICAL MODELLING AND SHAPE OPTIMIZATION OF COMPOSITE GIRDER WITH ADHESIVE BONDLINE

Paweł Szeptyński, Dorota Jasińska, Leszek Mikulski

Cracow University of Technology, Faculty of Civil Engineering Division of Structural Mechanics and Material Mechanics, Cracow, Poland

corresponding author Paweł Szeptyński: e-mail: pawel.szeptynski@pk.edu.pl

The paper presents a beam theory for composite girders consisting of two beams joined together with an adhesive layer. The height of the bottom beam is considered variable. The governing equations are suitable for formulation of a shape optimization problem in terms of control theory. The use of Pontryagin's maximum principle enables finding an optimal solution satisfying necessary optimality conditions. The presented optimization approach allows for including issues which cannot be accounted for by commercial topology optimization software. The introduced theory provides an estimated solution, which is then validated by an analysis of a 3D finite element model.

Keywords: composite beam theory, anisotropic limit state condition, structural optimization

1. Introduction

In recent decades, the use of composite structures has emerged as one of the most efficient solutions in structural engineering. Among a wide variety of distinct types of structures, those made of glue laminated timber (GLT) are especially suitable for structural optimization. Research devoted to this problem concerns shape optimization of load bearing elements (Mayencourt and Mueller, 2020; de Vito *et al.*, 2023), optimization of the structural layout (Hua *et al.*, 2020), combined shape and layout optimization (Šilih *et al.*, 2010; Kravanja and Žula, 2021) and also multiple aspects of optimal material usage (Mayencourt and Mueller, 2019; Pech *et al.*, 2019). With regard to composite structures exploiting advantageous mechanical properties of wood, a common solution is to combine solid wood or GLT girders with top reinforced concrete (RC) slabs – reviews on the topic of Timber-Concrete Composites (TCC) can be found in (Clouston and Schreyer, 2018; Dias *et al.*, 2018). The use of adhesive connections is still not a wide-spread approach in civil engineering, especially regarding the most heavily loaded bearing elements, as sufficiently precise modelling and technological issues are still a challenge. Various methods have been used to perform optimization tasks regarding timber structures, e.g. particle swarm optimization (Decker *et al.*, 2014), topology optimization (de Vito *et al.*, 2023) or genetic algorithms (Villar-García *et al.*, 2019). The making use of these methods does not guarantee that the obtained solutions satisfy necessary conditions of optimality. On the other hand, the use of Pontryagin's maximum principle (PMP) provides a solution that indeed satisfies the necessary conditions. The PMP is commonly used for solving one-dimensional control theory (CT) problems with a temporal independent variable. Its application to problems of structural optimization is thus restricted to one-dimensional problems of structural optimization, such as, e.g. optimization of rods and beams. Indeed, the PMP has been successfully applied to the problems

of optimization of cross-section of bar structures (Jasińska and Kropiowska, 2018; Jasińska and Mikulski 2019; Mikulski *et al.*, 2022; Szeptyński and Mikulski, 2023). Combining the simplified one-dimensional analytical model of a deformable solid with the general form of equilibrium equations in two dimensions enables an approximate description of a plane stress state. This is the approach used in the presented research. We shall consider a composite beam consisting of a top RC slab and a bottom GLT girder, which are connected by of an adhesive layer. The problem of shape optimization of the wooden girder is solved by means of the PMP, taking into account both serviceability and load carrying capacity constraints. The goal of this paper is to present a beam theory for composite girders and propose a useful method for determining nearly optimal shapes of such structures, which could not be found by of standard topology optimization techniques, due to specific problem conditions. Detailed engineering design is not the subject of this research as, in fact, there are still no regulations on the design of glued TCC structures, which is beyond the scope of the CEN/TS 19103. For these reasons and for the sake of simplicity of the presented numerical examples, the RC slab dimensioning, reinforcement specification, and cracking of the concrete are not taken into consideration – these issues might be, however, accounted for in a similar manner as other Eurocode regulations (Szeptyński and Mikulski, 2023). Among the novel contributions of the presented research to the current state-of-art, the following may be named:

- **Application an anisotropic limit state condition in optimization** – standard tools in topology optimization cannot take the anisotropic limit state condition into account, being restricted to the use of von Mises equivalent stress, which is applicable to isotropic solids only (Abaqus Tosca Structure, Ansys Structural Optimization). In both programs, it is also not possible to create such constraints with the user-defined responses. The PMP--based optimization does not suffer from these restrictions as it may take into consideration arbitrary nonlinear equality or inequality constraints.
- **Optimization within the regions with prescribed boundary conditions** – the topology optimization encounters problems when boundary conditions are prescribed in the design zone, since these conditions must propagate in some way to other nodes if some of them are removed. It is common to exclude the loaded and supported areas from the design zone (e.g. both in Tosca and Ansys). This approach usually leads to considerable overdimensioning of the structure in the supported zone. Contrary to this, the use of a simplified one-dimensional model enables optimization of the beam height along the whole length.
- **Numerical validation of results obtained via PMP-based optimization** – since the optimization by means of control theory requires a simplified one-dimensional model, validation of the obtained results has been performed with the use of a three-dimensional finite element model.

1.1. Scope of research

Three problems will be considered. The first one is derivation of governing equations and boundary conditions for the problem of bending of a composite beam with the bottom girder having variable height. These equations will then be transformed into a system of 1st order ODE, which suits the formalism of the PMP. The second task is solving the optimization problem for the considered single-span and double-span beams within the framework of the PMP. The problem is solved numerically by Dircol software which utilizes the direct collocation method. The third task is the validation of the obtained optimization results through a more detailed 3D Finite Element Method (FEM) numerical model. Finite element analysis (FEA) is performed with the use of Abaqus software.

2. Theoretical description

In the following Section, the theoretical background of the considered optimization problem will be presented. This includes an analytical model of a multilayer composite beam and an energy--based limit state condition for anisotropic materials exhibiting different strengths in tension and in compression. These equations will then be transformed in order to derive a system suitable for the application of Pontryagin's maximum principle.

2.1. Analytical model of a multilayer composite beam

The general theory of linear elastic multilayer composite beams, considered in this research, is derived and discussed in detail in (Szeptyński, 2020). A beam considered in this analytical model consists of a finite number of bent panels (beams) and sheared adhesive layers, placed in an alternating way. Deformation of the adhesive layers is assumed to be governed primarily by a simple shear state, while the bent panels are described within the Bernoulli-Euler beam theory. In the present research, the original statement of the problem is specified for the case of a three-layer beam (top slab + adhesive layer + bottom girder) and generalised in order to make it capable of taking into account variable height of the bottom panel.

2.1.1. Governing equations

We are considering a composite timber-concrete beam, the cross-section of which is shown in Fig. 1a. RC slab thickness is h_1 and width b_{pl} (which may be considered as the distance between neighbouring girders), as well as thickness of the adhesive layer is t and GLT girder width b. All parameters are fixed. The height of the bottom timber girder h_2 is the design variable.

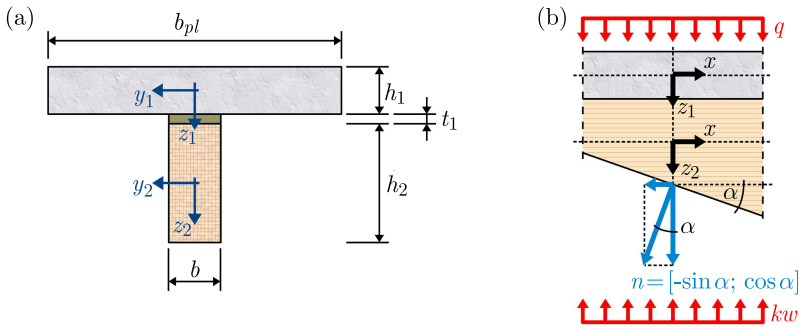

Fig. 1. a) Cross-section of the considered composite timber – concrete beam; b) Static boundary condition on the bottom face of the bottom beam

The derivation of a general form of governing equations from equilibrium equations, presented in (Szeptyński, 2020) is generalized here in a way enabling accounting for the variable height h_2 as well as bottom surface tractions representing contact stresses over the beam bearings, modelled by Winkler's subgrade, see Eq. (2.1). Besides, the method for including the static boundary conditions on the sloped bottom face of the beam is presented in the following Section. Linear elastic constitutive relations of Bernoulli-Euler beam theory are assumed for description of both the RC slab and the GLT girder. The kinematics of a pure shear state is used for description of deformation of the adhesive layer, in the same way as it is done in classical shear lag theories (Volkersen, 1938; Goland and Reissner, 1944). Due to relatively small thickness of the adhesive layer and slenderness of the layers in bending, transverse linear strain may be considered to be negligibly small. This justifies the assumption that the transverse displacement (deflection) is the same for both beam components. As a result, the following system of governing equations is obtained

$$
\begin{aligned}
&\frac{d}{dx}\Big(E_1A_1\frac{du_1}{dx}\Big)+G_1\frac{b}{t_1}\Big[(u_2-u_1)+\Big(\frac{h_1}{2}+\frac{h_2}{2}\Big)\frac{dw}{dx}\Big]=0\\
&\frac{d}{dx}\Big(E_2A_2\frac{du_2}{dx}\Big)-G_1\frac{b}{t_1}\Big[(u_2-u_1)+\Big(\frac{h_1}{2}+\frac{h_2}{2}\Big)\frac{dw}{dx}\Big]=0\\
&\frac{d^2}{dx^2}\Big[(E_1I_1+E_2I_2)\frac{d^2w}{dx^2}\Big]=\widehat{q}-kbw\\
&\quad+G_1\frac{b}{t_1}\Big\{\Big[\Big(\frac{du_2}{dx}-\frac{du_1}{dx}\Big)+\Big(\frac{h_1}{2}+\frac{h_2}{2}\Big)\frac{d^2w}{dx^2}+\frac{1}{2}\Big(\frac{dh_1}{dx}+\frac{dh_2}{dx}\Big)\frac{dw}{dx}\Big]\Big(\frac{h_1}{2}+\frac{h_2}{2}+t_1\Big)\Big\}\\
&\quad+G_1\frac{b}{2t_1}\Big\{\Big[(u_2-u_1)+\Big(\frac{h_1}{2}+\frac{h_2}{2}\Big)\frac{dw}{dx}\Big]\Big(\frac{dh_1}{dx}+\frac{dh_2}{dx}\Big)\Big\}
\end{aligned}
\tag{2.1}
$$

In formula (2.1), A_i and I_i stand for the area and 2nd moment of area of the cross-section of the i-th layer in bending ($i=1$ – RC slab; $i=2$ – GLT girder), respectively; E_i stands for Young's modulus of the material of the i-th bent layer and G_1 is Kirchhoff's modulus of the adhesive; k is the subgrade reaction coefficient describing stiffness of the bearing (outside the support area $k=0$); w, u_1 and u_2 are the common deflection of all layers and longitudinal displacements of the RC slab and GLT girder, respectively. Please note, that the governing equations depend only on one elastic constant of an anisotropic material, which makes an impression that the anisotropy is disregarded. This is an apparent inconsistency, since the beams under consideration are assumed to be slender enough so that the Bernoulli-Euler beam theory may be applied. As a result, both transverse shear deformation and transverse contraction are disregarded. As a consequence, the deflection of the beam is determined with just a single elastic constant. Such an approach is consistent with the use of the anisotropic limit state condition. The equivalent transverse load $\widehat{q}$ is defined as follows

$$\widehat{q}=q+(h_1g_1b_{pl}+h_2g_2b+t_1f_1b) \tag{2.2}$$

where q is the acting load, g_1, g_2 and f_1 are the specific weights of RC, GLT and adhesive, respectively.

2.1.2. Cross-sectional forces

The axial forces in the layers under bending are equal

$$N_1=E_1A_1\frac{du_1}{dx}\qquad N_2=E_2A_2\frac{du_2}{dx}\qquad N=N_1+N_2 \tag{2.3}$$

where N is the total axial force applied to the composite cross-section. The bending moment about the point P, placed in the distance Z_P from the top surface of the RC slab may be expressed as follows

$$
\begin{aligned}
M_P=&-\frac{b_{pl}E_1h_1^3+bE_2h_2^3}{12}\frac{d^2w}{dx^2}+E_1b_{pl}h_1\Big(\frac{h_1}{2}-Z_P\Big)\frac{du_1}{dx}\\
&+E_2bh_2\Big(h_1+t_1+\frac{h_2}{2}-Z_P\Big)\frac{du_2}{dx}
\end{aligned}
\tag{2.4}
$$

The formula for the transverse shear force – according to Schwedler's formula – after considering the equilibrium of axial forces, may be expressed in the following form

$$
\begin{aligned}
Q_P=&-\frac{1}{4}\Big(E_1b_{pl}h_1^2\frac{dh_1}{dx}+E_2bh_2^2\frac{dh_2}{dx}\Big)\frac{d^2w}{dx^2}-\frac{E_1b_{pl}h_1^3+E_2bh_2^3}{12}\frac{d^3w}{dx^3}\\
&+\frac{d}{dx}\Big(E_1A_1\frac{du_1}{dx}\Big)\frac{h_1}{2}+E_1b_{pl}h_1\frac{du_1}{dx}\frac{1}{2}\frac{dh_1}{dx}\\
&+\frac{d}{dx}\Big(E_2A_2\frac{du_2}{dx}\Big)\Big(h_1+t_1+\frac{h_2}{2}\Big)+E_2bh_2\frac{du_2}{dx}\Big(\frac{dh_1}{dx}+\frac{1}{2}\frac{dh_2}{dx}\Big)
\end{aligned}
\tag{2.5}
$$

2.1.3. Distribution of stress

Distribution of normal stress in bent layers is given by the following formulae

$$\sigma_{xx,i}(x,z_i) = E_i\Big(\frac{du_i}{dx} - \frac{d^2w}{dx^2}z_i\Big) \qquad i=1,2 \tag{2.6}$$

where $z_i \in (-h_i/2; h_i/2)$ is the distance from the centroid of the cross-section of the i-th layer in bending (Fig. 1a). The shear stress distribution in the adhesive layer is given by the following formula

$$\tau_a = \frac{G_a}{t}\Big[(u_2-u_1) + \Big(\frac{h_1}{2}+\frac{h_2}{2}\Big)\frac{dw}{dx}\Big] \tag{2.7}$$

The shear stress distribution in bent layers may be approximated with the use of Zhuravsky's formula, by integration of local equilibrium equations

$$\begin{aligned}
\sigma_{xz,1}(x,z_1) &= -\int\limits_{-\frac{h_1}{2}}^{z} \frac{\partial\sigma_{xx,1}}{\partial x}\,d\zeta = -E_1\Big[\frac{d^2u_1}{dx^2}\Big(z_1+\frac{h_1}{2}\Big) - \frac{1}{2}\frac{d^3w}{dx^3}\Big(z_1^2 - \Big(\frac{h_1}{2}\Big)^2\Big)\Big] \\
\sigma_{xz,2}(x,z_2) &= \tau_n - \int\limits_{\frac{-h_2}{2}}^{z} \frac{\partial\sigma_{xx,2}}{\partial x}\,d\zeta = \tau_n + E_2\Big[\frac{d^2u_2}{dx^2}\Big(\frac{h_2}{2}-z_2\Big) - \frac{1}{2}\frac{d^3w}{dx^3}\Big(\Big(\frac{h_2}{2}\Big)^2 - z_2^2\Big)\Big]
\end{aligned} \tag{2.8}$$

where τ_n is the shear stress at the bottom face of the GLT beam resulting from its slope. Let us denote the transverse normal stress at the bottom face of the GLT beam with p_n. The general static boundary condition for the bottom surface of the bottom layer, Eq. (2.9), enables finding the boundary shear stress (Fig. 1b)

$$\begin{bmatrix} \sigma_{xx,2}\Big(\frac{h_2}{2}\Big) & \tau_n \\ \tau_n & p_n \end{bmatrix}\begin{bmatrix} -\sin\alpha \\ \cos\alpha \end{bmatrix} = \begin{bmatrix} 0 \\ -kw \end{bmatrix} \quad \Rightarrow \quad \tau_n = \tan(\alpha)E_2\Big(\frac{du_2}{dx} - \frac{d^2w}{dx^2}\frac{h_2}{2}\Big) \tag{2.9}$$

Transverse normal stress in the layers in bending may be found by integration of local equilibrium equations

$$\frac{\partial\sigma_{xz,i}}{\partial x} + \frac{\partial\sigma_{zz,i}}{\partial z_i} + g_i = 0 \quad \Rightarrow \quad \sigma_{zz,i} = -\int\Big(\frac{\partial\sigma_{xz,i}}{\partial x} + g_i\Big)\,d\zeta + C_i \qquad i=1,2 \tag{2.10}$$

Since the through-the-thickness distribution of shear stress is quadratic, the transverse normal stress will be a cubic function of the z-coordinate

$$\sigma_{zz,1} = A_0 + A_1z_1 + A_2z_1^2 + A_3z_1^3 \qquad \sigma_{zz,2} = B_0 + B_1z_2 + B_2z_2^2 + B_3z_3^3 \tag{2.11}$$

Coefficients A_j, B_j $(j=0,1,2,3)$ are in fact functions of x, which are determined from the static boundary conditions and interface equilibrium conditions. The first four conditions are

$$\begin{aligned}
\sigma_{zz,1}\Big(-\frac{h_1}{2}\Big) &= -\frac{q}{b_{pl}} \qquad & \sigma_{zz,1}\Big(\frac{h_1}{2}\Big) &= p_{1,B} \\
\sigma_{zz,2}\Big(-\frac{h_2}{2}\Big) &= p_{2,T} \qquad & \sigma_{zz,2}\Big(\frac{h_2}{2}\Big) &= p_n
\end{aligned} \tag{2.12}$$

where $p_{1,B}$ and $p_{2,T}$ are the peel stresses at the bottom of the top layer (RC slab) and at the top of the bottom layer (GLT beam), respectively. They may be found from the equilibrium equation for transverse forces applied to the sheared layer

$$\begin{aligned}
p_{1,B} &= \frac{1}{b}\Big[\frac{d^2}{dx^2}\Big(E_1I_1\frac{d^2w}{dx^2}\Big) - \frac{d\tau_1}{dx}\frac{bh_1}{2} - \tau_1\frac{b}{2}\frac{dh_1}{dx} - q - h_1g_1b_{pl}\Big] \\
p_{2,T} &= p_{1,B} - G_1\Big[\Big(\frac{du_2}{dx} - \frac{du_1}{dx}\Big) + \frac{1}{2}\Big(\frac{dh_1}{dx} + \frac{dh_2}{dx}\Big)\frac{dw}{dx} + \Big(\frac{h_1}{2}+\frac{h_2}{2}\Big)\frac{d^2w}{dx^2}\Big] - t_1f_1
\end{aligned} \tag{2.13}$$

The normal stress p_n is determined according to (2.9)

$$p_n = \tan(\alpha)\tau_n - kw\sqrt{1+\tan^2(\alpha)} = \tan^2(\alpha)E_2\Big(\frac{du_2}{dx} - \frac{d^2w}{dx^2}\frac{h_2}{2}\Big) - kw\sqrt{1+\tan^2(\alpha)} \quad (2.14)$$

The remaining four conditions are derived from equilibrium equations, which determine the boundary values of derivatives of these distributions

$$\left.\frac{\partial\sigma_{zz,i}}{\partial z_i}\right|_{\pm\frac{h_i}{2}} = -\left.\frac{\partial\sigma_{xz,i}}{\partial x}\right|_{\pm\frac{h_i}{2}} - g_i \qquad i=1,2 \quad (2.15)$$

2.1.4. Boundary conditions

In order to determine the solution to equations (2.1) unambiguously, it is necessary to prescribe appropriate boundary conditions. The static boundary conditions on the top face of the RC slab and on the bottom face of the GLT girder are taken into consideration both in the governing equations and in the formulae for transverse normal stress. The sidewalls are assumed to be traction-free boundaries. The static boundary conditions are prescribed in an analogous way to classical beam theory as the conditions for end-values of cross-sectional forces.

2.2. Energy-based limit state condition for anisotropic materials with an asymmetric elastic range

A crucial aspect of the design of timber structures is the anisotropy of mechanical and strength properties of the material. It has been noted that in the case of slender beams, the anisotropy of elastic properties is of minor importance – it is not so regarding the strength properties of wood. An important feature is also the asymmetry of the elastic range, namely the difference between the limit values of tensile and compressive stress. Material properties corresponding with appropriate strength classes of structural timber can be found in the EN 338:2016 standard. However, standards regulating the structural design of timber structures may not specify any general approach to determine the ULS condition in the case of an arbitrary complex stress state. Only certain specific combinations of simple mechanical states are considered in the EN 1995-1-1:2010. In the considered optimization process, a general plane stress state is considered. For this reason, the energy-based limit state condition for orthotropic material exhibiting asymmetry of elastic range is used (Szeptyński, 2017)

$$F(\sigma) = A_I\sigma_I^2 + B_I\sigma_I + A_{II}\sigma_{II}^2 + B_{II}\sigma_{II} + A_{III}\sigma_{III}^2 \leqslant 1 \quad (2.16)$$

where projections of the current stress state on elastic eigensubspaces are equal

$$\sigma_I = \sigma_{11}\cos\kappa + \sigma_{22}\sin\kappa \qquad \sigma_{II} = -\sigma_{11}\sin\kappa + \sigma_{22}\cos\kappa \qquad \sigma_{III} = \sigma_{12} \quad (2.17)$$

The parameter κ is a function of the stiffness distributor. In (Szeptyński, 2017), one may find formulas for the parameter κ as well as coefficients A_I, A_{II}, A_{III}, B_I, B_{II}, expressed in terms of elastic constants and strength values. All these parameters can be found e.g. in the EN 338:2016, except for Poisson's ratio, however in the EN 1995-2:2004 it is allowed to take $\nu = 0$.

2.3. Formulation of the control theory problem

The optimization problem considered in this article may be stated as follows:
— minimize the total amount of GLT

$$V = \int_0^L A_2\,dx = b\int_0^L h_2\,dx \quad (2.18)$$

— subject to the following constraints
  – Ultimate Limit State (ULS) condition

$$F(\sigma) - 1 \leqslant 0 \tag{2.19}$$

  – Serviceability Limit State (SLS) condition

$$w_{max} - w_{adm} \leqslant 0 \tag{2.20}$$

where w_{max} is the maximum deflection, while w_{adm} is the maximum admissible deflection. The problem is meant to be solved with the use of Pontryagin's maximum principle. For this reason, the problem must be formulated in the form of a system of the 1st order ordinary differential equations (ODE). Let us introduce the following state variables

$$\begin{aligned}
&X_1 = u_1 \qquad X_2 = E_1 A_1 \frac{du_1}{dx} \qquad X_3 = u_2 \qquad X_4 = E_2 A_2 \frac{du_2}{dx} \\
&X_5 = w \qquad X_6 = \frac{dw}{dx} \qquad X_7 = (E_1 I_1 + E_2 I_2)\frac{d^2 w}{dx^2} \\
&X_8 = \frac{d}{dx}\Big[(E_1 I_1 + E_2 I_2)\frac{d^2 w}{dx^2}\Big] \qquad X_9 = h_2 \qquad X_{10} = \frac{dh_2}{dx} = \tan\alpha
\end{aligned} \tag{2.21}$$

We introduce a single control variable, namely

$$U_1 = \frac{d^2 h_2}{dx^2} \tag{2.22}$$

According to (2.18), the objective function is given by the integral functional stating the Lagrange optimization problem. It may be transformed into the Meyer optimization problem by introduction of an additional state variable and defining a new objective function J

$$X_{11}(x) = V(x) = b\int_0^x X_9(\xi)\, d\xi \quad \Rightarrow \quad J = X_{11}(L) \tag{2.23}$$

The new initial condition $X_{11}(0) = 0$ must be also prescribed. After this transformation, the governing equations take the following form

$$\begin{aligned}
&X_1' = \frac{1}{E_1 b_{pl} h_1} X_2 \qquad X_2' = -b\frac{G_1}{t_1}\Big[X_3 - X_1 + \Big(\frac{h_1}{2} + \frac{X_9}{2}\Big)X_6\Big] \\
&X_3' = \frac{1}{E_2 b X_9} X_4 \qquad X_4' = b\frac{G_1}{t_1}\Big[X_3 - X_1 + \Big(\frac{h_1}{2} + \frac{X_9}{2}\Big)X_6\Big] \\
&X_5' = X_6 \qquad X_6' = \frac{12 X_7}{E_1 b_{pl} h_1^3 + E_2 b X_9^3} \qquad X_7' = X_8 \\
&X_8' = q + h_1 g_1 b_{pl} + X_9 g_2 b + t_1 f_1 b - k b X_5 \\
&\quad + G_1 b\Big(\frac{h_1 + X_9}{2t_1} + 1\Big)\Big[\Big(\frac{1}{E_2 b X_9} X_4 - \frac{1}{E_1 b_{pl} h_1} X_2\Big) + \frac{6(h_1 + X_9)}{E_1 b_{pl} h_1^3 + E_2 b X_9^3} X_7 + \frac{1}{2} X_{10} X_6\Big] \\
&\quad + G_1 b\frac{X_{10}}{2t_1}\Big[X_3 - X_1 + \Big(\frac{h_1}{2} + \frac{X_9}{2}\Big)X_6\Big] \\
&X_9' = X_{10} \qquad X_{10}' = U_1 \qquad X_{11}' = b X_9
\end{aligned} \tag{2.24}$$

Cross-sectional forces and stresses may then be calculated according to equations (2.3)-(2.8) and (2.11) after expressing the derivatives of displacement functions in terms of the introduced state variables. The set of admissible values of the control variable is also defined. The final formal statement of the control theory problem is complex as the form of necessary optimality criteria depends on whether the constraints are active or not. The mathematical structure of a formulation of control theory problem subjected to PMP-based optimization may be found in (Mikulski *et al.*, 2022).

3. Numerical results

The single-span beam is assumed to be 15 m long with 40 cm at both ends resting on elastic supports. The double-span beam is assumed to be symmetrical, 28 m long, with two identical 14 m long spans, resting at both ends on 40 cm long elastic supports 40. The middle support is 60 cm long. The girder cross-sectional dimensions are assumed as follows: RC slab thickness $h_1 = 32$ cm, its width (distance between neighbouring GLT girders) $b_{pl} = 100$ cm, and the GLT beam width $b = 30$ cm. The adhesive layer is $t = 2$ cm thick. The elastic and strength properties of wood are adopted as for GL 26h, while mechanical properties of concrete are chosen as for C30/37 concrete class. The adhesive layer is assumed to be made of the SikaPSM flexible, virtually incompressible polyurethane adhesive, with Kirchhoff's modulus $G = 1.4$ MPa (Kwiecień, 2012; Śliwa-Wieczorek *et al.*, 2020). The total load applied to the beam includes the dead load of RC slab $g_1 = 25\,\mathrm{kN/m^3}$ and GLT girder $g_2 = 4.37\,\mathrm{kN/m^3}$ as well as the dead load of non-structural elements and live load, which together sum up to $q = 35\,\mathrm{kN/m^2}$. The subgrade reaction modulus is assumed to be equal to $k = 380\,\mathrm{MPa/m}$, as for an elastomeric support according to EN 1337-3:2005. In the supported section of the beam, the coefficients in the anisotropic limit state condition (2.16) are modified, namely, the compressive strength perpendicular to grain is increased by 75% according to Eurocode 5 recommendations 6.1.5 (2) and (3) of EN 1995-2:2007. Only a single load combination is considered, namely the one corresponding to uniform distribution of q, however the formulation of the problem and its solution may easily be expanded in order to account for multiple load combinations. The maximum admissible deflection is assumed to be $w_{adm} = L/250$. The range of admissible values of the control variable is $U_1 \in (-0.1; 0.1)$, while the height of the GLT beam itself may vary within the range $h_2 \in (0.3\,\mathrm{m}; 1.15\,\mathrm{m})$.

3.1. Results of the PMP-based optimization

The optimization problem stated in the previous Section is solved with the use of Dircol software. The results of completed optimization tasks for both analysed beams are presented in Figs. 2-4. Figures 2 and 3 illustrate the distributions of the GLT girders heights and deflections of optimal beams, respectively. The distribution of the magnitude of the left-hand side of the ultimate limit state criterion (material effort – see Eq. (2.17)) presented in Fig. 4, is plotted for five values of the z-coordinate, corresponding with the top, middle and bottom material fibres, as well as two additional intermediate coordinates.

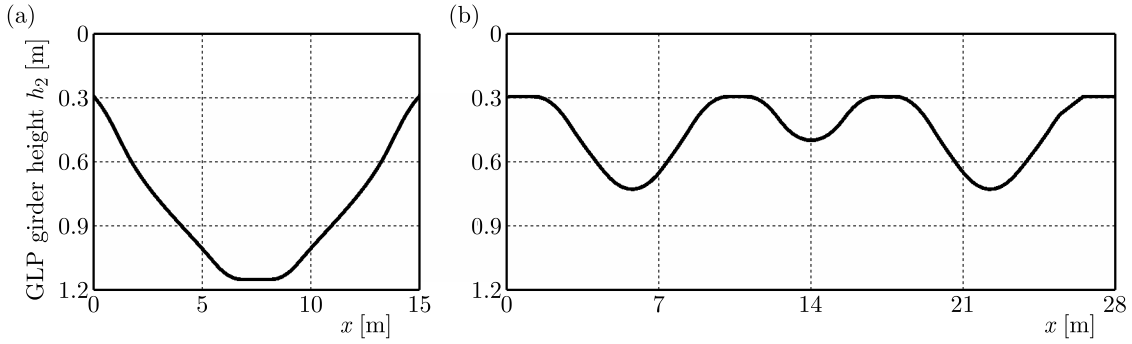

Fig. 2. Optimal distribution of the GLT girder height $h_2(x)$: (a) single-span beam, (b) double-span beam

An important feature of the obtained results is that in both analysed cases (the single and double-span beams) both SLS and ULS constraints are active. The highest material effort, activating the ULS constraints, appears at the bottom fibres ($z = 0,5h_2$) for both girders. It

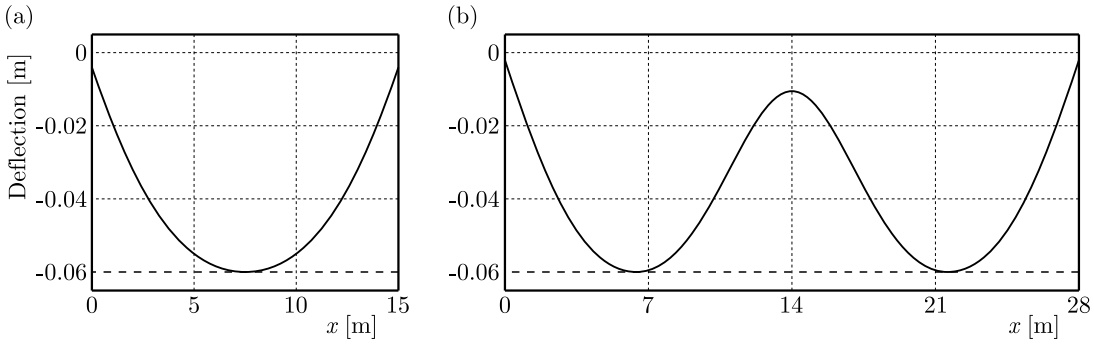

Fig. 3. Beam deflections with SLS: (a) single-span beam, (b) double-span beam

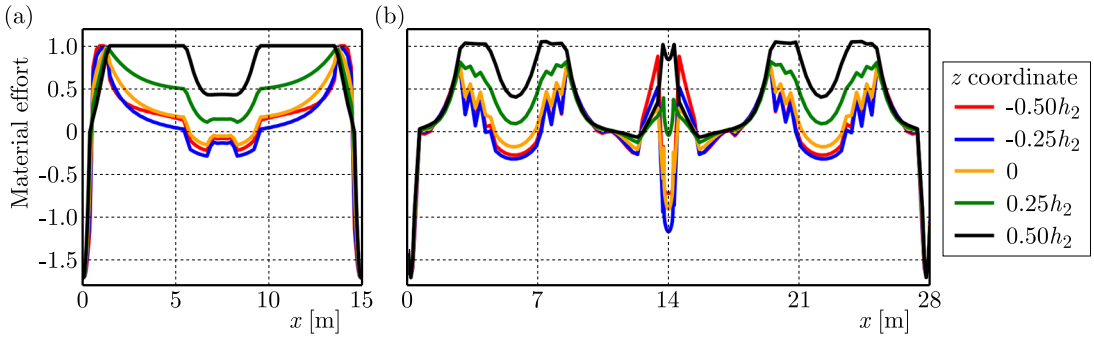

Fig. 4. Material effort: (a) single-span beam, (b) double-span beam

was observed that the acquired optimal control is singular, which means that the Hamiltonian of the system is piecewise constant. See Büskens *et al.* (2001) for a more detailed discussion.

3.2. Comparison with the 3D FE model

The optimal solutions obtained based on beam theory are compared with the results of a three-dimensional (3D) finite element analysis (FEA) performed with the use of Abaqus software.

3.2.1. Description of the FEM numerical model

The geometries of the 3D FEM girders models are assumed as follows: all cross-sectional and longitudinal beam dimensions, as well as material properties (span and support zone lengths) are the same as adopted for the above discussed 1D model (see the first paragraph of Section 3). The distributions of heights of the GLT girders (h_2) are taken from the results of the PMP based optimization (see Fig. 2). Both the concrete slab and GLT girder materials are assumed to be isotropic and linearly elastic. Since a pure shear elastic material model is not available in Abaqus, the adhesive is also assumed to be linearly elastic with $E_a = 4.14\,\text{MPa}$ and $\nu_a = 0.48$. The FEM mesh consists of linear hexahedral 8 node elements. The large number of used elements (over 100000) results from the necessity of precise modelling of the variable beam shapes, while keeping regular meshes, to obtain smooth stress maps along curved surfaces representing GLT fibres. The bearing supports are realized by applying linear vertical springs (with stiffnesses summing up to $k = 380\,\text{MPa/m}$) to nodes at the bottom girder surfaces in the support zones.

3.2.2. Comparison of results obtained with 1D beam and 3D FEA models

The distributions of displacements and stress tensor components found with the use of Dircol and Abaqus for both beams are compared in Figs. 5-9.

Since the bottom fibres of the GLT girder experience the highest stress levels (see Fig. 4), only these distributions are presented. The comparison of deflections of the single-span beam obtained by Dircol and Abaqus is presented in Fig. 5, whereas stress tensor components and measures of the material effort are compared in Fig. 6.

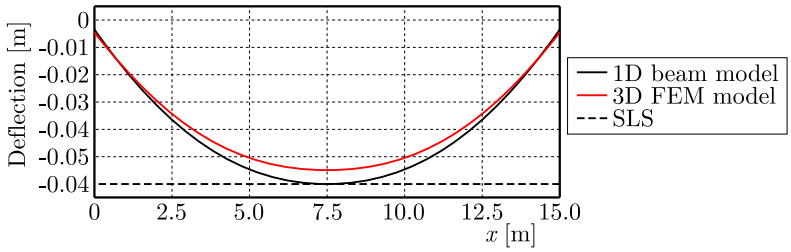

Fig. 5. Comparison of deflection of a single-span beam obtained from the 1D beam and 3D FEA models

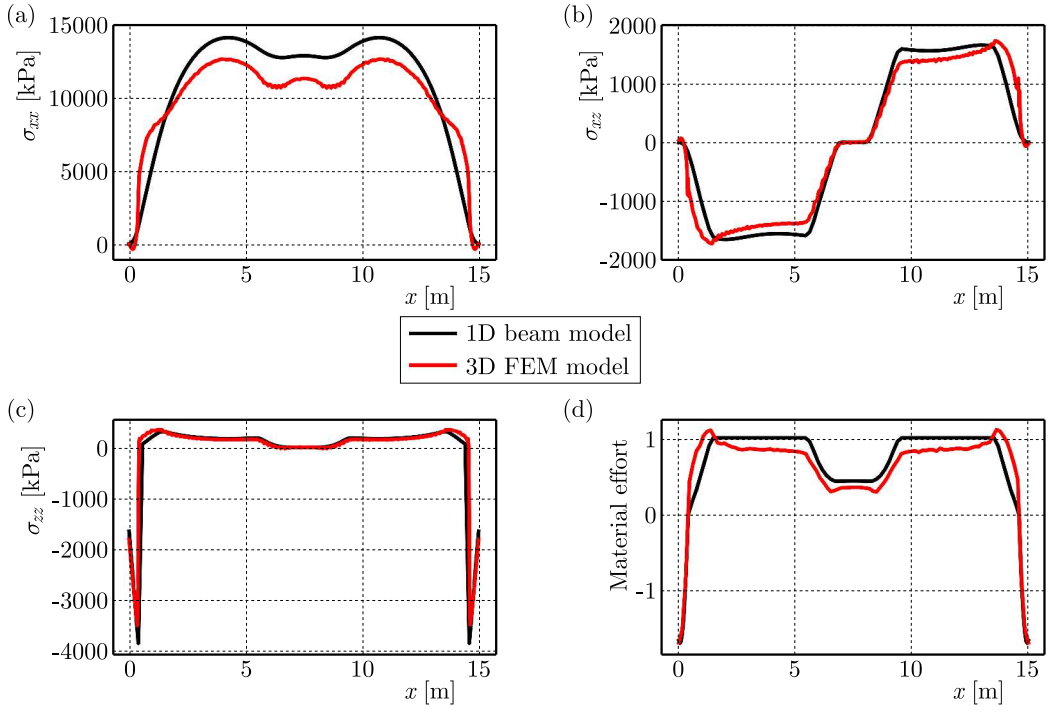

Fig. 6. Comparison of stress measures obtained from the 1D beam model and 3D FEA for bottom fibres of the GLT single-span beam: (a) axial normal stress, (b) shear stress, (c) transverse normal stress, (d) material effort

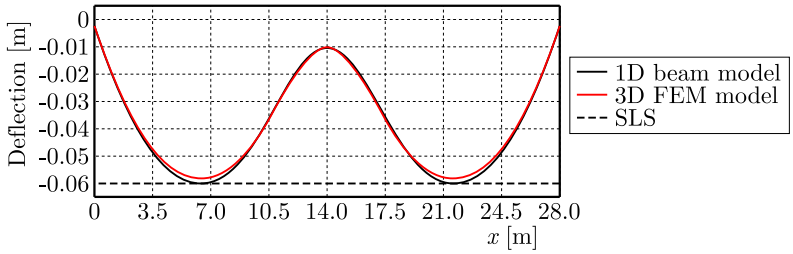

Fig. 7. Comparison of deflection of a double-span beam obtained from the 1D beam and 3D FEA models

Analogous comparisons of deflections and stresses obtained by Dircol and Abaqus for the double-span beam are collated in Figs. 7 and 8, respectively. Additionally, the distributions of shear stresses in the adhesive layers are compared in Fig. 9.

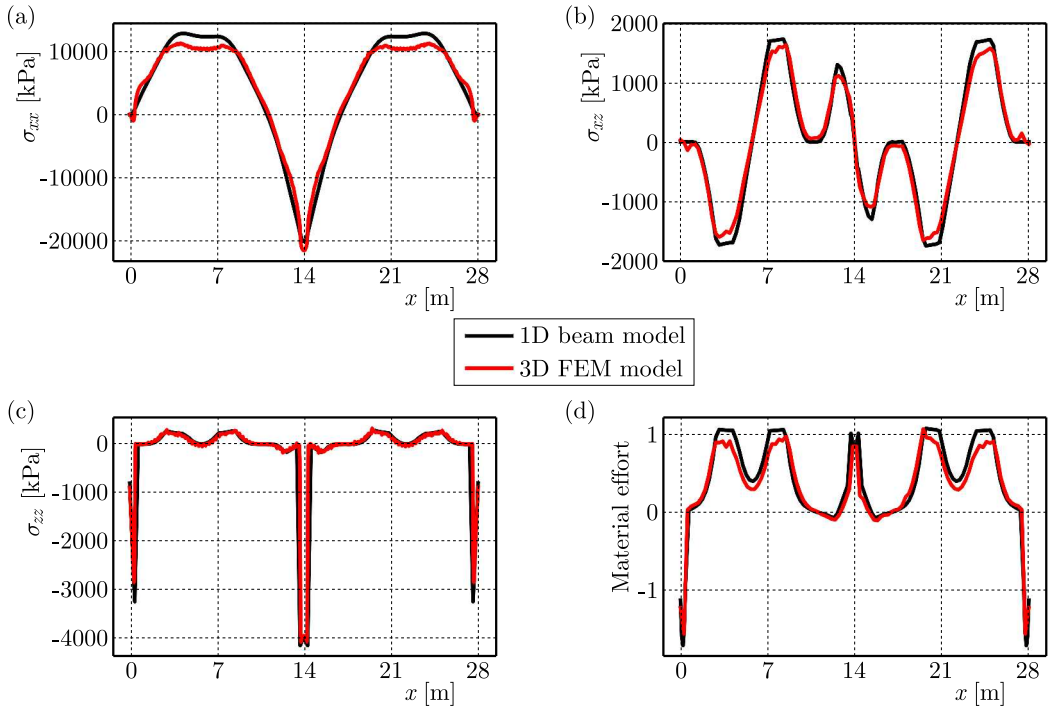

Fig. 8. Comparison of stress measures obtained from the 1D beam and 3D FEA models for the bottom fibers of the GLT double-span beam: (a) axial normal stress, (b) shear stress, (c) transverse normal stress, (d) material effort

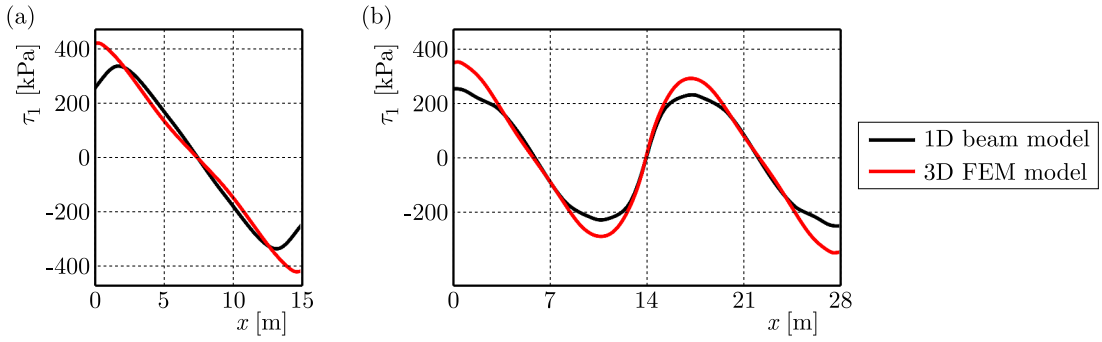

Fig. 9. Distribution of shear stress in the adhesive layer in (a) single-span beam, (b) double-span beam

4. Discussion

Analysing the comparison of stresses and deflections of optimal beams acquired with the 1D composite beam and 3D FEA models, under the same material assumptions (linear elasticity of all materials, isotropy of elastic constants of timber with the anisotropic limit state condition), presented in Section 3.2, one can note that:

- The 3D FEM model gives slightly smaller displacements (Figs. 5 and 7). Relative differences amount to 8% for the single-span beam and 4% in the case of the double-span beam.
- There is good agreement between the two models in stress distributions for both beams (Figs. 6 and 8). The ULS is active in these traction-free areas of the bottom fibres in both girders (Figs. 6d and 8d). Analysing the material effort in the 3D FEM model, one can notice that for the single-span beam the ULS is violated only pointwise by 2% (Fig. 6d) and is not exceeded in the case of the double-span beam (Fig. 8d).

- The greatest discrepancies between these two models concern the shear stresses in the adhesive layer (Fig. 9). This can be attributed to the simplifying assumption made in the 1D model according to which the adhesive layer undergoes simple shear deformation only, whereas in the FE analysis a general three-dimensional stress state is considered.
- One worrying result is the maximal deflection, which was greater for the 1D beam model than for the one obtained from the 3D FEA. One should expect that the 1D model, which is more severely constrained due to Bernoulli's hypothesis, should exhibit greater flexural rigidity. This result may be explained by the fact that in the simplified 1D model the longitudinal stiffness of the adhesive was completely disregarded as the adhesive was assumed to undergo simple shear only – in this sense this model is more compliant than the FEA model in which the three-dimensional stress and strain state is fully accounted for.

5. Summary and conclusions

The problem of shape optimization of a TCC beam with an adhesive layer has been stated. Governing equations have been derived, as well as expressions for cross-sectional forces and stresses. The problem has been reformulated in order to make it suitable for the application of Pontryagin's maximum principle. The optimization task has been carried out with the use of Dircol software for two composite beams – single and double span. Two constraint types have been considered: SLS condition restricting the maximum deflection and the ULS, which is formulated as a single inequality constraint making use of the energy-based estimate of the material effort for orthotropic materials exhibiting asymmetry in the elastic range. Both the ULS and SLS conditions are active in the obtained solutions. The observed discrepancies between the 1D beam theory solution and the results of 3D FEA indicate that the results obtained from the PMP-based optimization cannot be used without additional elaboration, however, the final shape may be easily found even by manual adjustment of the optimal solution obtained from the 1D beam model, according to the maps of the material effort.

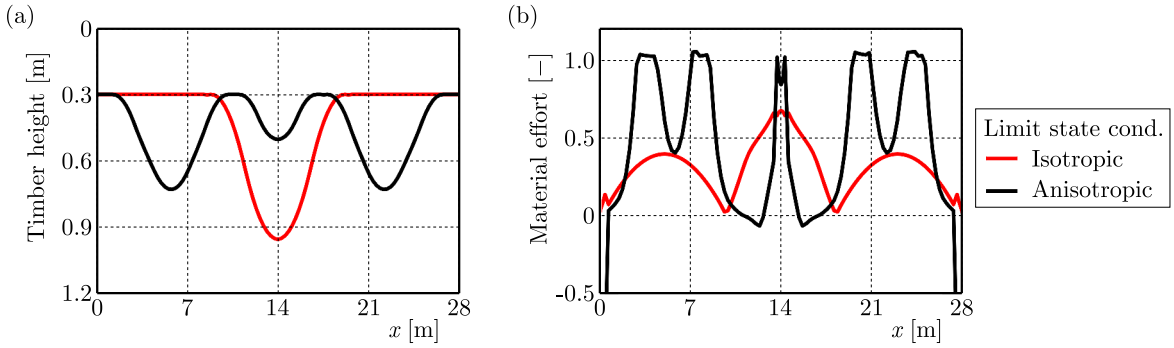

Fig. 10. Comparison of optimal double-span GLT girders obtained under isotropic and anisotropic limit state conditions: (a) height distribution, (b) material effort along bottom beam fibers

To estimate material savings achieved by shape optimization of the girders, the volumes of optimal beams have been compared with the volumes of composite beams with the same span lengths, loads and supports, but a constant GLT girder height. Minimal heights for which the SLS and ULS were not exceeded, and were adopted for this comparison. The relative material savings for the single-span beam are approximately 8%, while for the double-span beam 30%. An important conclusion arises when the anisotropy of the GLT is totally neglected in the task formulation, namely, when the timber is considered as an isotropic solid. Such an approach might be the first approximation in an optimization procedure. It can be shown that considerable errors

may occur when the anisotropy is not involved. In Fig. 10a, the optimal shape of the double-span beam obtained for the beam with the anisotropic limit state condition is compared with the one corresponding with the HMH condition (isotropic limit state condition).

In the case of the beam with the isotropic yield condition only the SLS constraint is active, wheteas if anisotropy is taken into account both SLS and ULS conditions are active (Fig. 10b). This is especially important when considering the fact that commercially available optimization programs offering topology or shape optimization often do not support anisotropy of strength properties (e.g. Tosca Structure). Even if anisotropy of elastic properties is taken into account, the fully stressed body optimization procedures can be governed only by isotropic limit state conditions such as the Huber-Mises-Hencky yield condition.

The performed analyses enable formulation of the following conclusions:

- The one-dimensional analytical model of a composite beam is suitable for application in the formalism of an optimization task of a control theory problem solved with the use of Pontryagin's maximum principle.
- A singular optimal solution may be found, for which both SLS and ULS constraints are active.
- Simplifications due to reduction of the dimension of the problem in the Bernoulli-Euler beam theory do not introduce significant errors neither in deformation nor in measure of the material effort.
- The results of the optimization of the 1D model need validation with the use of more accurate numerical models.
- The performed analyses prove that accounting for anisotropy of strength properties of the material and asymmetry of the elastic range play an important role in the optimization of timber beam structures. Failure to take into account for material anisotropy may lead to significant errors.

The proposed approach may readily be applied for shape optimization of composite beams with adhesive layers with any other support and load layout with multiple load cases taken into account.

References

1. Büskens C., Pesch H.J., Winderl S., 2001, Real-time solutions of bang-bang and singular optimal control problems, [In:] *Online Optimization of Large Scale Systems*, Springer-Verlag Berlin Heidelberg GmbH, 129-142
2. Clouston P., Schreyer A.C., 2018, Wood-concrete composites: a structurally efficient material option, *Civil Engineering Practice*, **21**, 1, 5-22
3. de Vito A.F., Vicente W.M., Xie Y.M., 2023, Topology optimization applied to the core of structural engineered wood product, *Structures*, **48**, 1567-1575
4. Decker S.A., Ndiaye A., Brangeon B., Sempey A., Galimard Ph., Pauly M., Lagiere Ph., Bos F., 2014, Design of multi-story timber building using mutli-objective particle swarm optimization, *Proceedings of the WCTE 2014 – World Conference on Timber Engineering*, **2**, 10-15
5. Dias A., Schänzlin J., Dietsch P., 2018, *Design of Timber-Concrete Composite Structures*, A state-of-the-art report by COST Action FP1402/WG4
6. Goland M., Reissner E., 1944, The stresses in cemented joints, *Journal of Applied Mechanics*, **11**, A17-A27
7. Hua H., Hovestadt L., Tang P., 2020, Optimization and prefabrication of timber Voronoi shells, *Structural and Multidisciplinary Optimization*, **61**, 1897-1911

8. Jasińska D., Kropiowska D., 2018, The optimal design of an arch girder of variable curvature and stiffness by means of control theory, *Mathematical Problems in Engineering*, **2018**, 1-13
9. Jasińska D., Mikulski L., 2019, Strength optimization of structural elements by means of optimal control, *MATEC Web of Conferences*, **262**, 10006
10. Kravanja S., Žula T., 2021, Optimization of a single-storey timber building structure, *International Journal of Computational Methods and Experimental Measurements*, **9**, 2, 126-140
11. Kwiecień A., 2012, Stiff and flexible adhesives bonding CFRP to masonry substrates – Investigated in pull-off test and Single-Lap test, *Archives of Civil and Mechanical Engineering*, **12**, 2, 228-239
12. Mayencourt P., Mueller C., 2019, Structural optimization of cross-laminated timber panels in one-way bending, *Structures*, **18**, 48-59
13. Mayencourt P., Mueller C., 2020, Hybrid analytical and computational optimization methodology for structural shaping: Material-efficient mass timber beams, *Engineering Structures*, **215**, 110532
14. Mikulski L., Jasińska D., Dąbrowska O., 2022, Structure of optimal control in optimal shaping of the steel arch, *Civil and Environmental Engineering Reports*, **32**, 3, 143-165
15. Pech S., Kandler G., Lukacevic M., Füssl J., 2019, Metamodel assisted optimization of glued laminated timber beams by using metaheuristic algorithms, *Engineering Applications of Artificial Intelligence*, **79**, 129-141
16. Šilih S., Kravanja S., Premrov M., 2010, Shape and discrete sizing optimization of timber trusses by considering of joint flexibility, *Advances in Engineering Software*, **41**, 2, 286-294
17. Śliwa-Wieczorek K., Zając B., Kozik T., 2020, Tests on the mechanical properties of polymers in the aspect of an attempt to determine the parameters of the Mooney-Rivlin hyperelastic model, *Civil and Environmental Engineering Reports*, **30**, 2, 1-14
18. Szeptyński P., 2017, Energy-based yield criteria for orthotropic materials, exhibiting strength--differential effect. Specification for sheets under plane stress state, *Archives of Metallurgy and Materials*, **62**, 2, 729-736
19. Szeptyński P., 2020, Comparison and experimental verification of simplified one-dimensional linear elastic models of multilayer sandwich beams, *Composite Structures*, **241**, 112088
20. Szeptyński P., Mikulski L., 2023, Preliminary optimization technique in the design of steel girders according to Eurocode 3, *Archives of Civil Engineering*, **69**, 1, 71-89
21. Villar-García J.R., Vidal-López P., Rodríguez-Robles D., Guaita M., 2019, Cost optimisation of glued laminated timber roof structures using genetic algorithms, *Biosystems Engineering*, **187**, 258-277
22. Volkersen O., 1938, Die Nietkraftverteilung in zugbeanspruchten Nietverbindungen mit konstanten Laschenquerschnitten, *Luftfahrtforschung*, **15**, 41-47

Manuscript received October 26, 2023; accepted for print November 30, 2023